Bioactive Materials 20 (2023) 306–317

Contents lists available at ScienceDirect

Bioactive Materials

journal homepage: www.keaipublishing.com/en/journals/bioactive-materials

Thiol-ene conjugation of VEGF peptide to electrospun scaffolds as potential application for angiogenesis

Tianyu Yao [a,b,1], Honglin Chen [c,1], Rong Wang [d], Rebeca Rivero [b], Fengyu Wang [e], Lilian Kessels [f], Stijn M. Agten [g], Tilman M. Hackeng [g], Tim G.A.M. Wolfs [f,h], Daidi Fan [a], Matthew B. Baker [b,*], Lorenzo Moroni [b,**]

[a] Shaanxi Key Laboratory of Degradable Biomedical Materials and Shaanxi R&D Center of Biomaterials and Fermentation Engineering, School of Chemical Engineering, Northwest University, Taibai North Road 229, Xi'an, Shaanxi, 710069, China
[b] Complex Tissue Regeneration Department, MERLN Institute for Technology Inspired Regenerative Medicine Maastricht University, Maastricht, 6229 ER, the Netherlands
[c] Guangdong Provincial People's Hospital, Guangdong Academy of Medical Sciences, Guangzhou, 510080, China
[d] Radboudumc, Department of Dentistry-Regenerative Biomaterials, Radboud University Medical Center, Philips van Leydenlaan 25, 6525 EX, Nijmegen, the Netherlands
[e] School of Medicine, South China University of Technology, Guangzhou, 510006, China
[f] Department of Pediatrics, Maastricht University Medical Center+, 6229 ER, the Netherlands
[g] Department of Biochemistry, Cardiovascular Research Institute Maastricht (CARIM), Maastricht University, 6229ER, the Netherlands
[h] School for Oncology and Developmental Biology (GROW), Maastricht University, Maastricht, the Netherlands

ARTICLE INFO

Keywords:
Electrospun
Fibrous scaffolds
Thiol-ene reaction
VEGF peptide

ABSTRACT

Vascular endothelial growth factor (VEGF) plays a vital role in promoting attachment and proliferation of endothelial cells, and induces angiogenesis. In recent years, much research has been conducted on functionalization of tissue engineering scaffolds with VEGF or VEGF-mimetic peptide to promote angiogenesis. However, most chemical reactions are nonspecific and require organic solvents, which can compromise control over functionalization and alter peptide/protein activity. An attractive alternative is the fabrication of functionalizable electrospun fibers, which can overcome these hurdles. In this study, we used thiol-ene chemistry for the conjugation of a VEGF-mimetic peptide to the surface of poly (ε-caprolactone) (PCL) fibrous scaffolds with varying amounts of a functional PCL-diacrylate (PCL-DA) polymer. 30% PCL-DA was selected due to homogeneous fiber morphology. A VEGF-mimetic peptide was then immobilized on PCL-DA fibrous scaffolds by a light-initiated thiol-ene reaction. 7-Mercapto-4-methylcoumarin, RGD-FITC peptide and VEGF-TAMRA mimetic peptide were used to validate the thiol-ene reaction with fibrous scaffolds. Tensile strength and elastic modulus of 30% PCL-DA fibrous scaffolds were significantly increased after the reaction. Conjugation of 30% PCL-DA fibrous scaffolds with VEGF peptide increased the surface water wettability of the scaffolds. Patterned structures could be obtained after using a photomask on the fibrous film. Moreover, *in vitro* studies indicated that scaffolds functionalized with the VEGF-mimetic peptide were able to induce phosphorylation of VEGF receptor and enhanced HUVECs survival, proliferation and adhesion. A chick chorioallantoic membrane (CAM) assay further indicated that the VEGF peptide functionalized scaffolds are able to promote angiogenesis *in vivo*. These results show that scaffold functionalization can be controlled via a simple polymer mixing approach, and that the functionalized VEGF peptide-scaffolds have potential for vascular tissue regeneration.

1. Introduction

Angiogenesis plays a pivotal role in tissue engineering and regenerative medicine for the successful survival of critical sized biological constructs [1–3]. During tissue regeneration, blood vessels can supply oxygen and nutrients to sustain cell viability [4,5]. Cells located

Peer review under responsibility of KeAi Communications Co., Ltd.
* Corresponding author;
** Corresponding author
E-mail addresses: m.baker@maastrichtuniversity.nl (M.B. Baker), l.moroni@maastrichtuniversity.nl (L. Moroni).
[1] Tianyu Yao and Honglin Chen contributed equally to this work.

https://doi.org/10.1016/j.bioactmat.2022.05.029
Received 10 June 2021; Received in revised form 7 May 2022; Accepted 23 May 2022

away from blood vessel suffer from hypoxia and apoptosis [6,7]. In the absence of blood vessels, the removal of cell waste products is limited, resulting in their local accumulation which trigger inflammatory responses [6,8]. A highly organized vascular network is required for engineered tissues.

To promote formation of vascular networks many strategies have been developed. One of the most promising approaches is the immobilization of growth factors or peptides on scaffolds to stimulate neovascularization [9]. Among those growth factors, vascular endothelial growth factor (VEGF) has been the most potential angiogenic promoter [10] by stimulating endothelial cell recruitment [11], proliferation [12,13], and differentiation [14], resulting in the formation of new blood vessels [15]. However, VEGF has not been applied widely because of its high costs, difficulties of manufacturing and the possibility of an adverse immune response [16,17]. An alternative approach has been to use VEGF-mimetic peptides [18–20]. To this end, D'Andrea et al. [21] designed a VEGF-mimetic peptide, QK (domain: KLTWQELYQLKYKGI), reproducing the helix region 17–25 of VEGF, and showed the ability to activate VEGF receptors with similar bioactivity to VEGF. QK peptides have provided many advantages over intact VEGF including smaller molecular weight, possibilities to use in chemical reactions, low immunogenic potential, and cost-effectiveness by synthesis [17,19–22]. This peptide promoted the attachment and proliferation of endothelial cells, and most importantly, induced capillary network formation [21,23]. Leslie-Barbick et al. also reported that the QK peptide is easier to conjugate or immobilize into poly(ethylene glycol) (PEG) hydrogels than VEGF because it could diffuse faster and more thoroughly into the scaffolds [20]. Yu and co-workers reported that covalently linked QK peptide within acrylate-PEG hydrogels enhanced vascular development, whereas addition of soluble QK peptide had no improvement when compared to unfunctionalized hydrogels [24]. This could be due to the free peptide quickly diffusing away from the scaffolds or fast proteolytic degradation. Their findings indicated that the immobilized QK peptide provided signals that direct endothelial cell migration and vascular ingrowth.

Scaffolds should be biodegradable, biocompatible and have native-like mechanical properties and a fibrillary structure that can mimic the structural and functional properties of the natural extracellular matrix (ECM) [8,25]. Significant progress has been made in the development of ECM-mimicking scaffolds for tissue engineering, primarily focusing on improving micro- and nano-fabrication techniques [26]. Among many scaffold fabrication methodologies, electrospinning has received much attention, due to the fact that it is a simple and effective polymer processing technique to produce micro and nanostructured fiber materials with a large surface to volume ratio [27–29]. By controlling the parameters of the electrospinning process, such as high voltage, flow rate and working distance, the morphologies, diameters and pore size of nanofibers can be successfully controlled [30,31]. The fibrillar structure of fibrous scaffolds with micro or nano diameter mimics the morphological features of ECM and provides a viable environment for cell adhesion, proliferation, migration, and differentiation [32,33]. Yang et al. has reported that loading QK peptide with electrospun poly(ethylene glycol)-b-poly(L-lactide-*co*-ε-caprolactone) (PELCL) scaffolds increased the proliferation of vascular endothelial cells during 9 days of culture [34]. Although physical loading is the most direct way to incorporate bioactive substances into nanofibrous scaffolds, the harsh conditions used during electrospinning could compromise the viability/stability of bioactive substances [35,36]. Besides, it is extremely difficult to homogeneously dissolve bioactives with high molecular weight in an organic phase for electrospinning process. Chew et al. investigated the possibility of loading human β-nerve growth factor (NGF) into electrospun poly(phosphoester) fibers [37]. Although sustained release of NGF was achieved, the protein was distributed randomly throughout the fibers in aggregate form due to phase separation between the organic polymer solution and the aqueous phases. Therefore, post functionalization could be another option to conjugate bioactives on electrsopun scaffolds.

Motivated by the versatile electrospinning approach for ECM mimicking micro/nano fibrous scaffolds fabrication and the unique contributions of VEGF-mimetic peptide in angiogenesis, we aimed to prepare electrospun VEGF peptide-functionalized PCL nanofibrous scaffolds to form bioactive scaffolds for vascular tissue engineering. Several methods can be found in literature describing the immobilization of a peptide to a targeted surface or scaffold, such as covalent conjugation chemistry [38–40] or the use of a crosslinker and binding tags [41,42]. However, many of these chemical reactions are nonspecific, possess limited efficiency and control and often require organic solvents that can compromise the activity of the bioactives or the mechanical stability of the scaffolds [22,43]. "Click" chemistry is an attractive alternative because of the simple reaction conditions, high reaction rate, high yields and functional group tolerance [44–46]. Several "click" methods including radical thiol-ene [47], copper-catalyzed azide alkyne cycloaddition (CuAAC) [48,49], strain-promoted azide–alkyne cycloaddition (SPAAC) [50,51], Diels−Alder addition [52] and Michael additions [53] have been employed for nanofiber modifications [54]. Wang et al. functionalized DC-ECMs with QK peptide via CuAAC click. The attachment of the QK peptide on to DC-ECM further enhanced the formation of branched tubular networks of endothelial cells [55]. The thiol-ene reactions also provide an attractive and effective method for functionalization due to the relatively mild reaction conditions and the ease of incorporation of thiols into functional peptides. Thiol-ene modification of electrospun meshes has previously been utilized for modification of polymers before and after spinning [56], and a few reports have shown the ability to graft functional peptides (RGD and YIGSR) directly after electrospinning [57,58]. Furthermore, the UV-initiated thiol-ene reaction has been shown to allow for facile photopatterning of an active polymer layer [47].

Here, we used thiol-ene chemistry to introduce VEGF-mimetic peptide on electrospun scaffolds. In the present work, we 1) synthesized "ene"-containing polymer with low molecular weight (PCL-diacrylates; PCL-DA; Mn ≈ 2000 g/mol), blend it with a high-molecular-weight PCL (Mn ≈ 8,0000 g/mol) for the fabrication of the functionalizable electrospun fibers; 2) designed thiol containing peptides to test the fidelity of the reaction; 3) applied the radical thiol-ene reaction to immobilize VEGF-mimetic peptides on the fibrous scaffolds; 4) cultured human umbilical vein endothelial cells (HUVECs) on the functionalized scaffolds and determined the VEGF-peptide signaling capacity of the scaffolds. Additionally, we carried forward to investigate the *in vivo* vascularization potential of these scaffolds using the chick chorioallantoic membrane (CAM) assay.

2. Materials and methods

2.1. Materials

Poly(ε-caprolactone) (PCL, Mn ≈ 80,000 g/mol), Poly(ε-caprolactone) (PCL-2k, Mn ≈ 2000 g/mol), trimethylamine, acryloyl chloride, 7-Mercapto-4-methylcoumarin and all organic solvents were purchased from Sigma Aldrich and used without further purification.

2.2. Synthesis of PCL-diacrylates (PCL-DA)

PCL-2k diol (4 g, 2 mmol) was dissolved in 40 mL of benzene and then reacted with 0.63 mL (7 mmol, 3.5 equiv) of trimethylamine and 0.37 mL (4.6 mmol, 2.3 equiv) of acryloyl chloride. The mixture was stirred at 80 °C for 3 h in a 250 mL three-necked flask, after which the triethylamine hydrochloride was removed by filtration. Finally, the mixture was precipitated in n-hexane and dried in a vacuum at 40 °C under reduced pressure for 24 h to produce the powdered form of PCL-DA. The final product was characterized by ^{1}H NMR and stored at −20 °C until use.

2.3. Synthesis of TAMRA-labeled VEGF mimetic peptide

VEGF-TAMRA mimic (TAMRA-GGCGGKLTWQELYQLKYKGI-$CONH_2$) was synthesized by manual solid-phase peptide synthesis on a 0.10 mmol scale using the *in situ* neutralization/activation procedure for Boc-/Bzl-peptide synthesis as previously described [59], but using HCTU instead of HBTU as a coupling reagent. MBHA resin (Sunresin, 1.07 mmol/g) was used as the solid support. TAMRA is referred as 5-carboxytetramethylrhodamine. After completion of the peptide chain, the resin-bound peptide was washed with dimethylformamide (DMF) and treated with trifluoroacetic acid (TFA) (2 × 1 min) to remove the N-terminal Boc group. 6-carboxytetramethylrhodamine-Succinimidyl ester (AAT Bioquest, 1.1 eq in 400 μL DMF) was added to the resin bound peptide and left to react for 2 h at 37 °C. The completed peptide chain was washed with DMF, CH_2Cl_2 and 1:1 *v/v* CH_2Cl_2/MeOH, and subsequently dried until further use.

The peptide was deprotected and cleaved from the resin by treatment with anhydrous HF for 1 h at 0 °C, using 4 *v*-% *p*-cresol as a scavenger. Following cleavage, the peptide was precipitated in ice-cold diethyl ether, dissolved in 50% water/50% acetonitrile containing 0.1% TFA, and lyophilized. After lyophilization the peptide was purified by semi-preparative HPLC. Fractions containing the desired product were identified by UPLC-MS, pooled and lyophilized.

In order to test the specificity of the thiol-ene reaction, the free thiol at the cysteine residue was alkylated in a portion of the purified peptide. The peptide was dissolved in 50 mM ammonium bicarbonate, pH 8 and was reduced by incubation with DTT (20 mM) for 1 h at 37 °C for. Subsequently, the reduced peptide was alkylated by addition of iodoacetamide (40 mM) and reacting for 30 min protected from light at room temperature. The alkylation reaction was quenched by addition of DTT (20 mM). The reaction was monitored by MALDI-TOF-MS and the desired product was purified by semi-preparative HPLC. Fractions containing the desired product were identified by UPLC-MS and pooled. The final peptide concentration of the pooled fraction was measured by absorbance at a wavelength of 550 nm using a Varian Cary 50 BIO UV-VIS Spectrophotometer.

2.4. VEGF-TAMRA mimic peptide characterization

UPLC-MS was performed on a Waters XEVO QTOF G2 Mass Spectrometer, with an Acquity H-class solvent manager, FTN-sample manager and TUV-detector. The system was equipped with a reversed phase C18-column (Waters, Acquity PST 130A, 1.7 μm 2.1 × 50 mm i.d.), column temperature 40°. Mobile phases consisted of 0.1% formic acid in water (solvent A) and in 90% acetonitrile (solvent B). FTN-purge solvent was 10% acetonitrile in water. Gradient condition: 10%–55% solvent B over 15 min monitored at 220 nm.

Semi-Preparative reversed-phase HPLC was performed on a Waters Delta Prep System equipped with a Waters 2487 Absorbance Detector, using a Vydac C-18 column (250 × 10 mm, 10 μm). A linear gradient of acetonitrile in water/0.1%TFA was used to elute the peptide. Flowrate was 12 mL/min. Finally, Matrix-Assisted Laser Desorption/Ionization Time-of-Flight (MALDI TOF)-MS was performed on an Applied Biosystems 4800 MALDI TOF/TOF system in reflector mode using α-cyano-4-hydroxycinnamic acid as matrix material. Both peptides were isolated as single peaks in the LC/MS analysis with VEGF-TAMRA giving an observed mass of 664.34 $[M+4H]^{4+}$ (expected 664.53) and VEGF-TAMRA-alk giving an observed mass of 678.57 $[M+4H]^{4+}$ (expected 678.79), with *m/z* ratios resulting in a monoisotopic mass of 2652.28 (expected 2652.33) and 2709.28 (expected 2709.35), respectively.

2.5. Preparation of electrospun PCL-DA fibers

A high molecular weight of PCL and a lower molecular weight of PCL-DA were blended in different ratios (10, 30, and 50 wt % of PCL-DA as described in Table S1) to give a final concentration of 20 wt % polymer in a solvent mixture, respectively. All polymer solutions were prepared in chloroform-dimethylformamide ($CHCl_3$:DMF = 4:1). The electrospinning parameters were selected based on previous study [60]. After mixing properly, PCL solution was transferred into a 5 mL syringe capped with a stainless steel blunt-ended nozzle. The syringe was connected with a silicon feed line to deliver polymer solution, then equipped into a syringe pump with a fixed flow rate at 1 mLμμ/h. The steeμ needle was set 20 cm from aluminum plate. A high voltage of 20 kV was then used during electrospinning. The temperature was kept at 25 °C.

2.6. Characterization of electrospun fibers

The morphology of the PCL-DA electrospun fibers was observed by scanning electron microscopy (SEM; XL30; Philips). The diameter of electrospun fibers were determined by Image J. The morphological change of the fibers after binding with thiol-ene reaction was also examined.

2.7. Fluorescent dye immobilization on fibers using thiol-ene reaction

7-Mercapto-4-methylcoumarin was used to validate thiol-ene reaction with 30% PCL-DA fibrous scaffolds. The fibrous mesh was covered with 1 mL of ethanol-water (1:1) solution containing 7-Mercapto-4-methylcoumarin (2 mg/mL) in a petri dish. The petri dish was exposed to UV light for 10 min (365 nm, intensity 10 mW/cm^2). The control group was treated in dark for the same time. After the reaction, the sample was washed with excess ethanol-water (1:1) solution to remove the unbound dye. Fluorescence was observed with a fluorescent microscope (Nikon Eclipse Ti–S) and then quantified by UV–Vis spectrophotometer (UV–Vis Cary60; Agilent). Each of the absorption bands were monitored by Fourier-transform infrared spectroscopy (ATR-FTIR; Bruker). The variation in molecular weight of 30% PCL-DA was determined from gel permeation chromatography (GPC). GPC measurements were carried out on a Shimadzu Prominence-i LC-2030C 3D equipped with a refractive index detector and a photodiode array detector, using a Shodex KD-G 4A guard column (4.6 × 10 mm) with 8 μm beads, two Shodex KD-802 (5 μm, 8 × 300 mm) and KD-804 (7 μm, 8 × 300 mm) columns. N,N-dimethylformamide (DMF) containing 0.1 wt % LiBr as stabilizing agent was used as eluent and samples of 2 mg/mL at a constant flow rate of 1 mL min-1 at 50 °C was applied. The GPC system was calibrated with poly(methyl methacrylate) (PMMA) standards.

Patterning solutions consisted of 2 mg/mL 7-Mercapto-4-methylcoumarin in an ethanol-water (1:1) solution. 30% PCL-DA fibrous scaffolds containing the desired solution were covered with different photomasks and irradiated for 10 min. Patterned fibrous mesh were placed in ethanol-water (1:1) solution and washed 3 times to remove the excess dye. Fluorescence pattern was visualized by a UV lamp.

2.8. Functionalization of PCL-DA fibrous scaffolds with fluorescent peptides

RGD-FITC peptide (CGGGRGDSK-FITC) (MW: 1339 g/mol; China-Peptides) and VEGF TAMRA mimic peptide (TAMRA-GGCGGKLTWQE-LYQLKYKGI-$CONH_2$) were used to validate the thiol-ene reaction between peptides and PCL-DA scaffolds. The peptides were dissolved in ethanol-water (1:1) solution at a concentration of 2 mg/mL. The PCL-DA (10 and 50%) fibrous scaffolds was placed in the peptide solution along with or without a photoinitiator (Irgacure 2959, 0.5 w/v%) at room temperature during 30 min. This fibrous scaffolds were then exposed to 10 mW/cm^2 UV for 10 min. After that, the electrospun scaffolds were washed several times with ethanol-water (1:1) until all of the non-reacted peptide was removed. Scaffolds fluorescence was observed with a fluorescent microscope (Nikon Eclipse Ti–S) and then quantified by UV–Vis spectrophotometer (UV–Vis Cary60; Agilent).

2.9. Functionalization of PCL-DA fibrous scaffolds with VEGF peptide and VEGF-TAMRA peptide

VEGF peptide (Ac-CGGKLTWQELYQLKYKGI-NH_2) (MW: 2090.35; ChinaPeptides) or VEGF-TAMRA peptide (MW: 2652.28 was dissolved in ethanol-water (1:1) solution at a concentration of 2 mg/mL. The 30% PCL-DA fibrous scaffolds was placed in the peptide solution along with a photoinitiator (Irgacure 2959, 0.5 w/v%) at room temperature. This fibrous scaffold was then exposed to 10 mW/cm^2 UV for 10 min. The active form of the peptide bonded onto PCL-DA fibers is termed as "30% PCL-DA/VEGF pep" fibrous scaffolds.

2.10. Mechanical test and contact angle measurements

The mechanical behavior of PCL-DA and PCL-DA-peptide electrospinning fibers was carried out on a DMA tester (Q800, TA corporation, USA) at room temperature. Typically, electrospinning fibers with a rectangular shape (length: 20 mm, width: 6 mm, height: 0.25 mm) were fixed with two stainless steel clamps and stretched at a constant rate of 50% strain/min. The tensile stress of the electrospinning fibers was calculated according to the following description: stress = $F \times L/A_0 \times L_0$, where F, L, A_0, and L_0 represent the force, the real-time length between clamps, initial cross-sectional area, and initial length of sample, respectively. Strain was defined as $(L\text{-}L_0)/L_0 \times 100\%$. The elastic modulus was calculated from the slope of linear segment from 0% to 5% strain by the tensile stress-strain curve.

The water contact angle of different scaffolds was measured using the sessile drop method. For this measurement, the scaffolds were fixed on the plate of a contact angle device (OCA15, Dataphysics, Germany). 4 μL of water drop was released on the surface of the scaffolds through a syringe. Images of the liquid drop on the scaffolds were captured for the calculation of the water contact angle.

2.11. Cell culture

HUVECs were purchased from Lonza and cultured in endothelial growth medium (EGM, Lonza) containing EBM™-2 basal medium (CC-3156) and EGM™-2 SingleQuots™ supplements (CC-4176). HUVECs between four and eight passages were used in this study. The culture medium was changed every 2 days and the cells were cultured at 37 °C in a humidified 5% CO_2.

All electrospun scaffolds (diameter: 15 mm) were disinfected by 70% ethanol for 30 min and then dried under a biosafety flow hood. The disinfected scaffolds were placed on a 24-well plate and fixed by O-rings (ERIKS).

2.12. Cell survival on different scaffolds

After washing with sterilized water, the scaffolds were coated using Matrigel® (1:150 dilution in EBM) overnight in order to increase cell attachment. HUVECs (2×10^4) were then seeded on the scaffolds, and incubated with 5% CO_2 at 37 °C. To evaluate cell survival on 30% PCL-DA and 30% PCL-DA/VEGF pep fibrous scaffolds, endothelial basal media (EBM) without growth factors was used to induce a starvation condition. After seeding on scaffolds, cells were cultured in a growth-factor-free setting for cell viability and DNA assays. Cell viability was tested by the PrestoBlue™ reagent (Fisher Scientific). Briefly, at 1, 3, and 5 days after cell seeding, 500 μL of PrestoBlue medium at a dilution of 1:10 with EBM media were added to each sample and incubated at 37 °C with 5% CO_2. 30 min later, 100 μL of media were placed into 96-well plate to measure absorption value at a wavelength of 590 nm using a microplate reader (CLARIOstar, BMG Labtech). DNA content of cell-scaffolds was evaluated with CyQUANT™ Cell Proliferation Assay Kit (Thermo Fisher Scientific) according to the manufacturer's protocol. The cells harvested after 1, 3, and 5 days were washed with PBS and digested overnight with 250 μL Proteinase K in Tris/EDTA solution at 56 °C. After freeze-thawing samples for 3 times, the digested solutions were then transferred into a black 96-well plate. A 40 μL of lysis buffer was added into each well and incubated for 1 h. Finally, the cell lysate was stained with 80 μL GR dye for 15 min at room temperature. Fluorescent intensity was measured at an excitation/emission of 450/520 nm using microplate reader. A standard curve of DNA content was obtained using serially diluted λDNA with the concentration ranging from 0 to 1 μg/mL. No Matrigel pre-coating on both scaffolds was also performed on cell survival assay. However, cells were dead rapidly in EBM on non-treated scaffolds.

2.13. Cell proliferation on different scaffolds

Cell viability and proliferation were tested by the Cell Counting Kit-8 (CCK-8, Dojindo, Japan) kit and CyQUANT™ Cell Proliferation Assay Kit. The cell proliferation on 30%PCL-DA and 30%PCL-DA/VEGF pep fibrous scaffolds was evaluated by using endothelial growth media without VEGF (EGM-VEGF) to assess the specific effect of VEGF peptide. No Matrigel pre-coating on both scaffolds was performed in this assay. First, HUVECs (2×10^4) were seeded on the scaffolds, and incubated with 5% CO_2 at 37 °C. After 1 day, 3 days and 5 days culture, 500 μL of CCK8 solution were added to each sample and incubated for 3 h. After that, 100 μL of culture solution were placed into a 96-well plate, and the optical density (OD) was measured at a wavelength of 450 nm using a microplate reader. Cell proliferation on scaffolds was evaluated by CyQUANT™ Cell Proliferation Assay Kit to measure the total DNA content on scaffolds. The experiment procedure was similar as described above. Tris(2-carboxyethyl)phosphine (TCEP) is a commercially reducing agent to break Cys-Cys bridge, and used as co-reactant for the thiol-ene reaction of 30% PCL-DA fibrous scaffolds with VEGF peptide. We compared cell survival on VEGF peptide functionalized scaffolds with and without TCEP catalyst. No differences were observed (data not shown). Therefore, TCEP was not added into reaction solution in the following experiment.

2.14. VEGFR1 and VEGFR2 phosphorylation ELISA assays

The concentrations of phosphorylated VEGF receptor 1 (VEGFR1) and VEGF receptor 2 (VEGFR2) were assayed by using Human Phospho-VEGFR1 and Human Phospho-VEGFR2 DuoSet IC ELISA kits (R&D Systems). First, HUVECs were seeded on 30% PCL-DA and 30% PCL-DA/VEGF pep fibrous scaffolds, then cultured in EGM without VEGF medium. HUVECs seeded on 30% PCL-DA scaffolds cultured in EGM with VEGF (20 ng/mL) was referred to as a control condition in the experimental set-up. After incubating 2 h and 4h, HUVECs were washed with PBS 2 times. Cells were solubilized in lysis buffer following the recommended protocol from R&D. 100 μL of sample and controls were added to the pretreated 96-well plates and incubated for 2 h at room temperature. After washing with wash buffer, 100 μL of detection antibody conjugates were added and placed under dark for 2 h. The well plate was carefully aspirated and washed by wash buffer. A 100 μL of substrate solution was added to each well and incubated for 20 min in the dark. The reaction was ended by adding 2 N H_2SO_4. A plate reader was used to determine the optical density in each well at a wavelength of 450 nm.

2.15. Cell morphology on fibrous scaffolds

Cell adhesion morphologies on different scaffolds were observed. Briefly, the cell-scaffolds were fixed with 4% Paraformaldehyde at 4 °C overnight, and then dehydrated using a graded series of ethanol (30%, 50%, 70%, 80%, 90%, 96% and 100%). After immersed in 500 μL hexamethyldisilazane (HMDS, Sigma–Aldrich) for 30 min twice, cell-scaffolds were placed in dry air overnight. Dehydrated samples were finally sputtered with gold and then were examined by an ultra-high resolution FE-SEM (MERLIN, ZEISS).

2.16. Chick chorioallantoic membrane assay

To assess the bioactivity and angiogenesis of functionalized scaffolds *in vivo*, the chick embryo chorioallantoic membrane (CAM) assay has been performed. Briefly, fertilized Lohman white leghorn eggs (provided by Het Anker B.V., Netherlands) were placed in an incubator (n = 10 for each condition) at day 0 and kept under 50–55% humidity at 37 °C and rotated once every hour. Eggs were rotated during the first 3 days of incubation to prevent attachment of the embryo to the eggshell. After 3 days of incubation, a square window of 1 × 1.5 cm^2 was opened in the eggshell with a saw (Dremel) and then sealed with scotch tape to prevent dehydration. On day 10, uncoated VEGF peptide functionalized scaffolds with diameter of 4 mm were placed on the surface of the chorioallantoic membrane. On day 14, the vessels surrounding the scaffold was visualized under a Leica DM5 microscope. A change in vessel number and vessel area around fibrous scaffolds was quantified by using Image J. This change in vascularization implies an effect of functionalized scaffolds on angiogenesis *in vivo*.

2.17. Statistical analysis

Statistical analysis was performed by GraphPad Prism 8 software. All data are shown as mean ± standard deviation (SD). Data were statistically analyzed by one-way analysis of variance; column values were compared with the control values using Student's t-test. A probability value of less than 0.05 was considered significantly different. Levels of significance were as follows: *P ≤ 0.05, **P ≤ 0.01, ***P ≤ 0.001.

3. Results and discussion

3.1. Characterization of PCL-diacrylates (PCL-DA)

PCL-diacrylate was synthesized via treatment of PCL-diol (2 kDa) with acryloyl chloride. The reaction was straightforward, and the formation of PCL-diacrylate (49% acrylation degree) was confirmed through ^{1}H NMR spectrometer. As shown in ^{1}H NMR spectrum (Fig. S1), the CH_2=CH- signals of the PCL-diacrylate was present in the δ 5.80–6.45 ppm range, which is consistent with other literature [61–63]. The detail of vinyl groups is shown below: ^{1}H NMR (700 MHz, $CDCl_3$) δ 6.41 (dd, J = 17.4, 1.1 Hz, 1H), 6.13 (dd, J = 17.3, 10.4 Hz, 1H), 5.83 (dd, J = 10.5, 1.1 Hz, 1H). From the ^{1}H NMR results, the hydroxyl groups in PCL were successfully converted to vinyl groups of PCL-DA after reacting with acryloyl chloride.

3.2. Fabrication of PCL-DA-Incorporated electrospun PCL fibers

To investigate the effect of PCL-DA (2 kDa) on fiber morphology, different percentages of PCL-DA were incorporated into PCL solution and the concentrations of the total polymer solution was fixed to be in 20% (Table S1). The morphology of the formed fibrous scaffolds was observed by SEM (Fig. 1). With higher percentage of PCL-DA, the fibrous scaffolds displayed smaller fibers. After more PCL-DA was added, the average dimeter of PCL fibers decreased from 1.71 ± 0.18 to 0.49 ± 0.23 μm (Fig. S2a), suggesting that the diameter of PCL fibers decreased after mixing with lower molecular weight PCL-DA. Moreover, 10% PCL-DA and 30% PCL-DA fibrous scaffolds showed more uniform fiber morphology compared to 50% PCL-DA scaffolds. 30%PCL-DA fibers showed much more narrow distribution of fiber diameter compared with the other two scaffolds (Figs. S2b–d). Our finding that fiber diameter decreases with the decline of molecular weight was also studied in literature. Tao et al. reported that at a fixed concentration, the polyvinylalcohol (PVA) fiber diameter decreased as the molecular weight was decreased [64]. When the molecular weight decreased, the solution viscosity decreased significantly. During the electrospinning process, the low surface tension produced by the low viscosity of the polymer solution could result in smaller fibers.

3.3. Surface modification of PCL-DA fibers

The availability of functionalizable groups on the fiber surfaces was demonstrated using a thiol-containing fluorescent dye, 7-mercapto-4-mehtylcoumarin (Fig. S3). Fluorescence images were captured from the 30% PCL-DA fibers after thiol-ene reaction in the solution of 7-mercapto-4-methylcoumarin. Compared to the reaction groups, the fluorescence in the controls was much weaker. The results demonstrated successful modification with 7-mercapto-4-methylcoumarin onto PCL-DA fibrous scaffolds (Fig. S3b). Fluorescence labeling of 30% PCL-DA fibers with thiol dye proved that the -ene groups were available for thiol-ene coupling. The success of fluorescence dye coupling was further verified via FTIR spectroscopy. The "C=C" stretch peak (~1625 cm^{-1}) was not visible after reaction (Fig. S3c purple line), while much stronger signals of benzene (~1590 cm^{-1}) were found after functionalization,

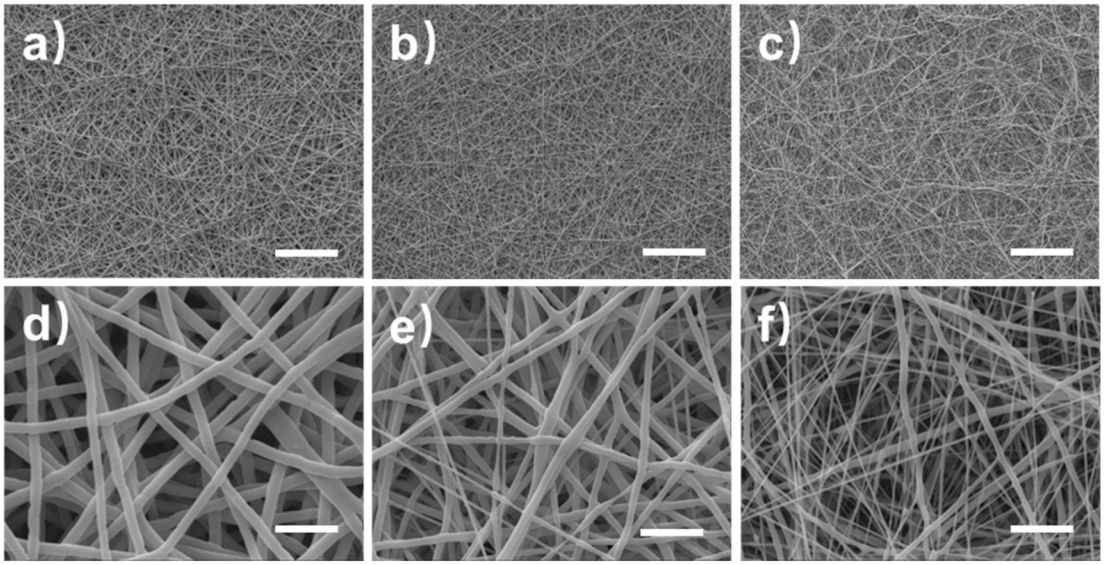

Fig. 1. Micro- or nano-structure of electrospun fibrous scaffolds; (a and d) 10% PCL-DA, (b and e) 30% PCL-DA, and (c and f) 50% PCL-DA at low (top) and high (bottom) magnifications. Scale bars are 100 μm (a–c) and 10 μm (b–d).

indicating the complete conversion of the -ene groups within the limits of FTIR detection. These results support a successful thiol-ene event where a C–S–C linkage is formed between PCL-DA and 7-mercapto-4-methylcoumarin. Conjugation of fluorescence dye to PCL-DA fibrous scaffolds was also investigated via GPC (Fig. S4a), which demonstrated that there were no major changes in the polymer molecular weight composition before and after the thiol-ene reaction. The images on the right are PDA traces of the GPC on the left. A strong signal of reacted 30%PCL-DA fibrous scaffolds from GPC-coupled PDA detector at 335 nm (Fig. S4b) was observed. The strong spots in the absorption spectrum around 335 nm at retention times of ~15 min corresponded to the successful coupling of 7-mercapto-4-methylcoumarin to the lower molecular weight 2K PCL-DA. This is another confirmation that the chemistry we designed is the chemistry that is working and operational in the system.

The thiol-ene chemistry results with a fluorescence dye proved that "functionalizable" groups on the fiber surface are also available for further thiol-ene functionalization. Unlike many functionalization methods, this blend and thiol-ene reaction does not need specific solvents which may destroy the morphology of fibers. Therefore, this surface functionalization approach provides an opportunity to couple VEGF mimicking peptides, among other biological factors, on the surface of PCL-DA fibers without interfering with the fiber morphology.

3.4. The effect of time and PCL-DA concentration on thiol-ene reaction

After reacted with 7-mercapto-4-methylcoumarin, the fluorescence intensity of fibrous scaffolds was quantified by UV–Vis spectrophotometer. As shown in Fig. 2a, with increasing of the reaction time, the fluorescence intensity increased rapidly at first until 10 min and then further increased gradually reaching a relative high point after 30 min. Besides, the use of long exposure time for the reaction may lead to photobleaching. Therefore, 10 min was chosen as the effective reaction time for further investigation. Without the UV exposure, the control group showed no specific absorbance, indicating that the PCL-DA were intact during this process and no obvious physical absorption was found in this 30 min treatment. The absorbance intensity of the test line depended on the yield of the thiol-ene conjugation of 7-mercapto-4-methylcoumarin, which in turn corresponded to the reaction site of PCL-DA scaffolds. Although photobleaching may influence the photochemical reactions of fluorescein, this method gave an indication on which exposure time is enough for the reaction.

By dissolving functionalized scaffolds, we could quantify the amount of dye conjugated to the surface with a calibration curve (Fig. S5). In Fig. 2b, it can be seen that the amount of 7-mercapto-4-methylcoumarin immobilized on the surface increased with increased blend ratio of PCL-DA, with 10% and 30% giving similar amounts of coupled dye. Clearly, higher mixing ratio of PCL-DA lead to the greater amount of surface -ene, which provided more functional group for fluorescence dye or peptide coupling on the surface. Especially, 50% PCL-DA scaffolds contained many smaller fibers with diameter around 490 nm, some fiber diameter even decreased below 200 nm. It was reported that as fiber diameter decreases, the specific surface area increases dramatically and a much higher fiber surface could be exposed to activation [65,66]. Higher surface area could lead to a higher reaction site, which is related to a significant increase in bonding 7-Mercapto-4-methylcoumarin. This result showed the possibility to control the reaction by changing the percentage of PCL-DA. Although the 50% PCL-DA fibrous scaffolds contained the highest amount of functionalizable groups, the obtained fiber diameters were quite small and less uniform compared with 30% PCL-DA scaffolds. Finally, 30% PCL-DA fibrous scaffolds were chosen for subsequent *in vitro* and *in vivo* studies.

3.5. Photopatterning of PCL-DA fibrous scaffolds

To demonstrate UV-regulated the process of fiber functionalization, we performed photopatterning experiments to generate fluorescence patterns using photo masks (Fig. 3a). This photopatterning strategy is based on the advantage of using the photochemically promoted radical thiol-ene reaction, so that conjugation of 7-mercapto-4-methylcoumarin under UV exposure through a photomask was probed. Fig. 3b showed the resulting fluorescent pattern after thiol-ene reaction on 30% PCL-DA fibrous scaffolds, where the bright-blue regions are areas of reacted polymer fluorescing under UV light. Black regions were masked during reaction and remained unfunctionalized. As a demonstration, various patterns were achieved on the 30% PCL-DA fibrous scaffolds by UV illumination through different photomasks (Fig. 3c). The photopattern approach based on thiol-ene reaction was also reported by other researchers [47]. However, this study did not show the possibility of performing photopatterning on fibrous scaffolds. Our study successfully proved that this simple and effective approach could be used on PCL-DA fibrous scaffolds. The ability to use thiol-ene chemistry creating any spatial functionalization of PCL-DA fibrous films is a significant advantage, which could later be used for the partial functionalization of bioactive molecules on fibrous scaffolds.

The mixing approach of PCL-DA with PCL in our study not only gives

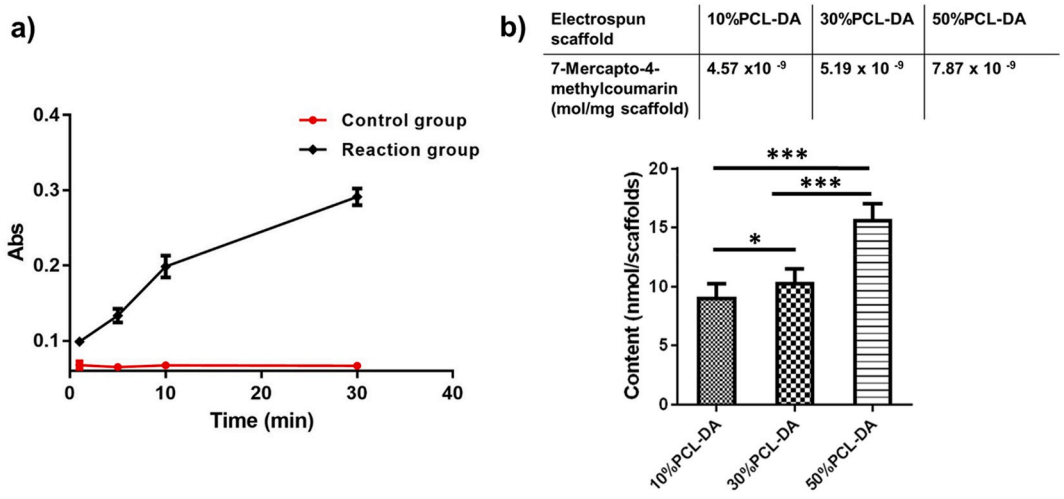

Electrospun scaffold	10%PCL-DA	30%PCL-DA	50%PCL-DA
7-Mercapto-4-methylcoumarin (mol/mg scaffold)	4.57×10^{-9}	5.19×10^{-9}	7.87×10^{-9}

Fig. 2. (a) The effect of reaction time on the fluorescence increases of 30% PCL-DA fibrous scaffolds. The control group is the reaction group without UV treatment. Excitation wavelength: 335 nm. (b) Quantification of 7-Mercapto-4-methylcoumarin reacted with per 10, 30 and 50% of the PCL-DA electrospun scaffolds, respectively. (*$P \leq 0.05$, ***$P \leq 0.001$; $n = 3$).

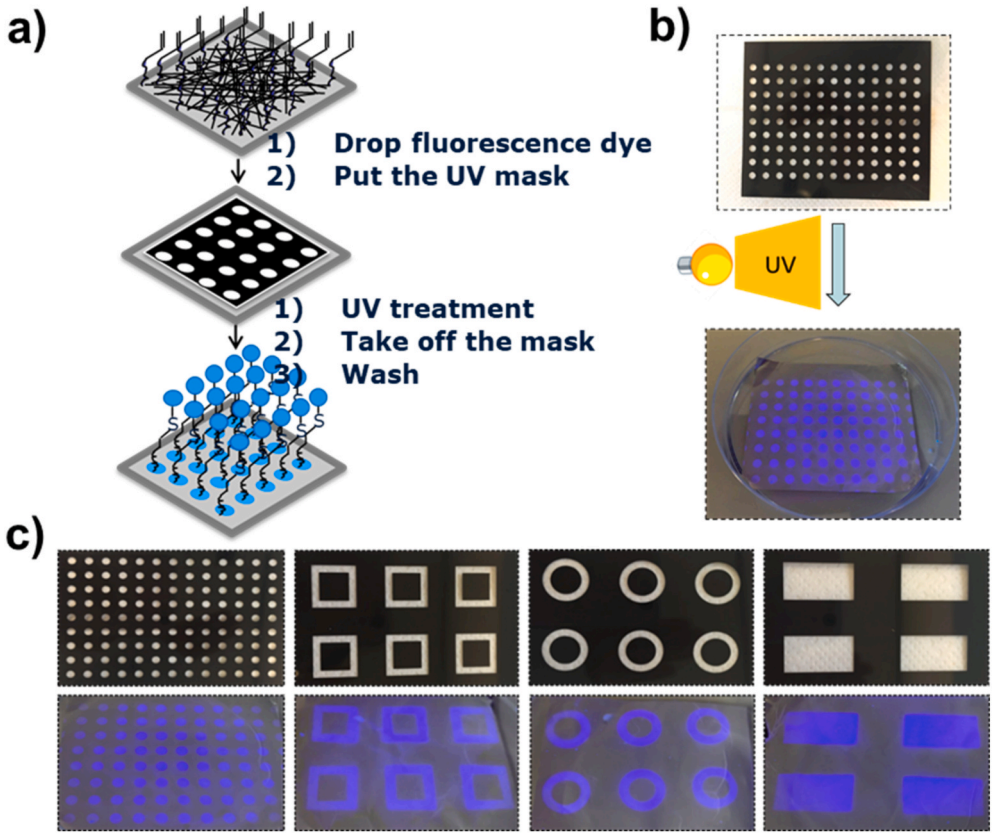

Fig. 3. (a) Photopatterning steps of 30%PCL-DA fibrous scaffolds with 7-Mercapto-4-methylcoumarin. (b) Images of mask and photopatterned fibrous scaffolds and (c) different mask and photopatterned fibrous scaffolds.

the ability to control the functionalization of scaffolds, but also shows the possibility to pattern scaffolds. Spatial control of functionalization could guide the distribution of bioactive molecules on scaffolds, which provide specific cues for the generation of well-organized vascular networks in tissue regeneration. This approach could be further used to improve the angiogenic potential of synthetic scaffolds in the future.

3.6. PCL-DA scaffolds functionalization with fluorescent peptides

To probe the ability of the scaffolds to be functionalized with a bioactive peptide, we initially tested RGD-FITC construct (Fig. S6). Showing that the reaction was successful via fluorescence microscopy, we turned to creating fluorescently labelled VEGF peptide mimetics to test the fidelity of the reaction with appropriate model reactions. In this experiment, we wanted to determine the range of peptide functionalizations possible with this approach, and chose to study further the 10% and 50% functionalized fiber scaffolds. A VEGF-TAMRA was created via solid phase Boc peptide synthesis, with an installed TAMRA dye connected to a spacer remote to the cysteine reactive site. Conveniently the peptide synthetic methodology also allowed us to create a VEGF-TAMRA with an alkylated cysteine, thus blocking the available thiol for the thiol-ene reaction (VEGF-TAMRA-alk). VEGF-TAMRA mimetic peptides were characterized by HPLC/MS and both showed single peaks after purification with the corresponding expected masses (Fig. S7).

Fig. 4a showed the resulting fluorescence after the reaction of VEGF-TAMRA on two electrospun scaffolds with different concentrations of

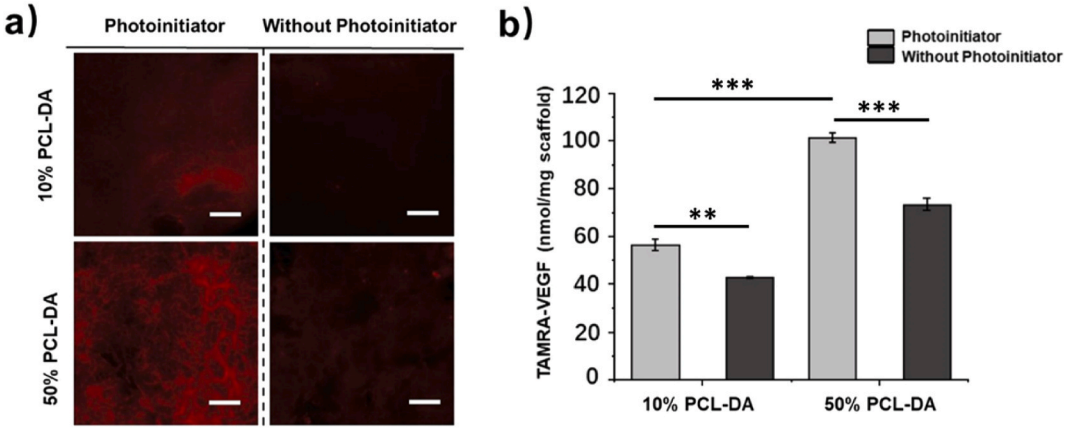

Fig. 4. (a) VEGF-TAMRA mimic peptide immobilizing on different PCL-DA electrospun scaffolds. Up: 10% PCL-DA scaffolds; Down: 50% PCL-DA scaffolds. (b) Quantification of VEGF-TAMRA concentration in the different electrospun scaffolds. Scale bars are 100 μm. (**P ≤ 0.01, ***P ≤ 0.001; n = 3).

PCL-DA (10 and 50%). The amount of the immobilized VEGF-TAMRA mimic peptide was increased in the material with higher amounts of DA groups. A low amount of fluorescence was observed in the controls without photoinitiator. This is likely due to either small amounts of the thio-Michael addition occurring during these treatments [67], or due to the low concentration of free-radicals which can be generated by UV-light alone.

VEGF-TAMRA-alk mimic peptide with a blocked cysteine was used to verify that the occurring reaction involves the addition of a thiol to an alkene to form the alkyl sulfide. No significant differences in the fluorescence intensity of the different scaffolds (10 and 50% PCL-DA) at different conditions (with and without photoinitiator) could be observed when the reactive cysteine group was blocked (Fig. S8). The fluorescence observed in these images can be attributed to a small amount of physical absorption of the TAMRA on the PCL-DA.

The concentration of VEGF-TAMRA mimic peptide in the different scaffolds was calculated from a calibration curve of TAMRA in DMF (Fig. S9). The concentration per mg of scaffold increased with the number of functional groups on the surface available for peptide coupling (Table S2) and was estimated at 56.5 and 101.4 nmol/mg of scaffold for the 10% and 50% PCL-DA scaffolds (Fig. 4b), respectively. Although the functionalization of the scaffold with the peptide could also occur in the absence of the photoinitiator, the fluorescence intensity observed of the thiol-ene reaction was approximately 30% higher with initiator. Photobleaching may reduce fluorescence of VEGF-TAMRA, while the changes of fluorescence between different groups are still evident.

3.7. Mechanical properties and contact angle of different scaffolds

The mechanical properties of 30% PCL-DA and 30% PCL-DA/VEGF pep fibrous scaffolds were investigated. As shown in Fig. 5a, the ultimate strain and tensile strength of 30% PCL-DA/VEGF pep fibrous scaffolds were ~181% and ~2.72 MPa, respectively, which were significantly higher than those of 30%PCL-DA fibrous scaffolds (~138% and ~0.15 MPa). The modulus of elasticity was shown to be significantly different between the two different scaffolds (Fig. 5b). The moduli for 30% PCL-DA/VEGF pep fibrous scaffolds was 7998 ± 1824 kPa, whereas the 30%PCL-DA fibrous scaffolds showed a lower modulus of 4041 ± 1085 kPa. The results of stress–strain curves and elastic modulus indicated that the mechanical properties of 30% PCL-DA/VEGF pep fibrous scaffolds increased higher than that of 30% PCL-DA fibrous scaffolds. This can be explained by the fact that the functionalization process (UV exposure with initiator) of VEGF peptide on 30% PCL-DA fibrous scaffolds initiates crosslinking between or within PCL-DA fibers, possibly resulting in stiffer mechanical properties. After functionalization with VEGF peptide, SEM images showed that the PCL-DA fibers maintained their fiber morphology (Figs. S10a–b). This observation indicated the crosslinking of PCL-DA and the functionalization with VEGF peptide did not change the morphology and diameter of PCL-DA fibers (Fig. S10c). Moreover, the hydrophilicity of the 30% PCL-DA fibrous scaffolds was increased after the functionalization with VEGF peptide comparable to unfunctionalized 30% PCL-DA scaffolds. The 30% PCL-DA fibrous scaffolds provided a water contact angle of 121 ± 3.3°, while functionalization with VEGF peptide resulted in a contact angle of 109 ± 1.2° (Fig. S10d). The possible explanation could be that the conjugation of VEGF peptide on PCL-DA fibers increased the hydrophilicity of 30% PCL-DA fibrous scaffolds, which could facilitate the attachment and penetration of cells.

3.8. HUVECs survival on 30% PCL-DA/VEGF pep scaffolds under starvation conditions

HUVECs were seeded on the Matrigel coated 30% PCL-DA and 30% PCL-DA/VEGF pep scaffolds under starvation medium to study the contribution of VEGF peptide on cell survival. Cell viability was evaluated by using the PrestoBlue assay at 1, 3 and 5 days. Fig. 6a indicates that cell viability on both scaffolds were similar at day 1. Cell viability for both scaffolds decreased after 3 days' incubation under starvation conditions, whereas no significant decrease was identified at day 5. In addition, cell survival was also determined using a CyQUANT™ Cell Proliferation Assay Kit to measure total DNA content. Results showed that DNA content for both groups gradually decreased over 5 days (Fig. 6b). The DNA content of both scaffolds was the same at day 1. After 3 days' culture under starvation medium, both scaffolds experienced extensive cell death. The DNA content at day 5 on the 30% PCL-DA scaffolds was 24.4% of its day 1 value, while it was 29.6% for the 30% PCL-DA/VEGF pep scaffolds.

The DNA content on VEGF peptide functionalized scaffold at day 1 was significantly higher than that on the control scaffold at day 3 and day 5, indicating that VEGF peptide on scaffolds increased HUVECs survival. These observations supported that VEGF peptide was successfully immobilized onto the scaffolds. Although the mechanical properties of 30% PCL-DA scaffolds changed after functionalization, the slightly change in moduli would not have influence on cells survival in the present study. Previous study reported that cells may be in response to changing substrate stiffness. Jalali et al. demonstrated that Young's Moduli of human umbilical vein endothelial cells (HUVECs) were 218.85 ± 38.73, 385.58 ± 131.67, and 933.20 ± 428.92 Pa for soft (65.01 ± 21.14 Pa), medium (770.83 ± 67.32 Pa), and hard substrates (1032.61 ± 82.78 Pa), respectively [68]. However, the Young's Moduli of scaffolds in the present study were 4041 ± 1085 kPa (without UV treatment) and 7998 ± 1824 kPa (with UV treatment), which value is far above the threshold moduli that cells could be response to. The cell

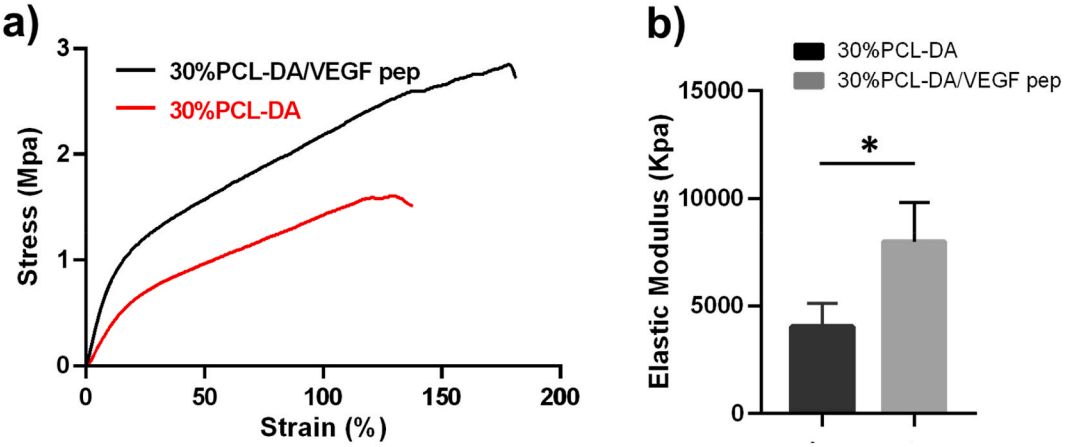

Fig. 5. Representative tensile stress–strain curves (a) and elastic modulus (b) of 30% PCL-DA and 30% PCL-DA/VEGF pep fibrous scaffolds. (*P ≤ 0.05; n = 3).

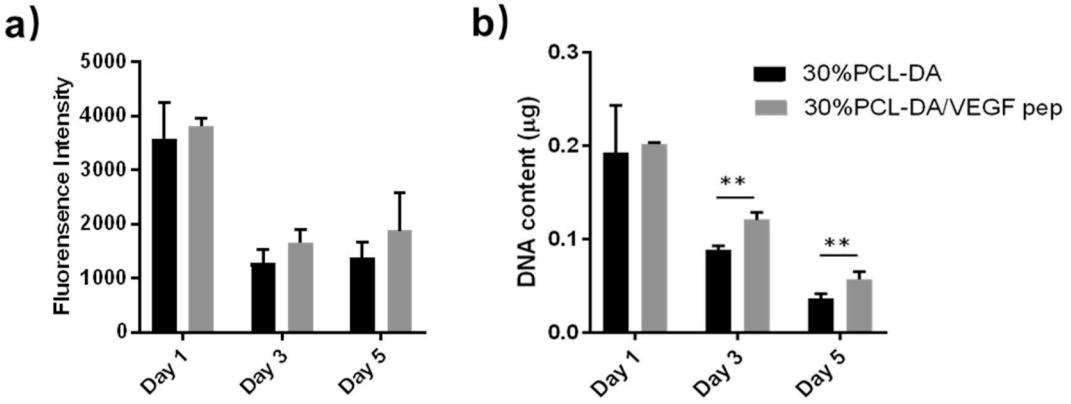

Fig. 6. Effect of VEGF peptide immobilizing on HUVECs survival under nutrient starvation conditions. Viability (a) and DNA content (b) of HUVECs cultured for 5 days on Matrigel coated 30% PCL-DA and 30% PCL-DA/VEGF pep fibrous scaffolds. (**P ≤ 0.01; n = 3).

stiffness reached a plateau of 7 kPa when the substrate stiffness was ~20 kPa, and the cells retained this stiffness even on essentially infinitely rigid substrates like glass [69]. Therefore, HUVEC survival is more likely related to the functionalization of the fibers with VEGF peptides rather than the difference in moduli. In the process of tissue transplantation, insufficient vascularization of the implantation site or poor angiogenesis at beginning could lead to cell death. Low cell survival is probably due to the nutrient starvation conditions. Efforts employing pro-survival growth factors or peptide functionalized scaffolds have been applied to increase cell survival. We suppose that using VEGF peptide scaffolds to prolong endothelial cell survival until forming vessel network might be a promising approach to improve the survival of transplanted tissue. HUVECs were also seeded on uncoated 30% PCL-DA and 30% PCL-DA/VEGF pep scaffolds to test cell survival. However, cells were dead rapidly in EBM on both uncoated scaffolds.

3.9. VEGFR1 and VEGFR2 phosphorylation assay on the scaffolds

In order to further detect biological signaling of VEGF peptide from the functionalized scaffolds, HUVECs were cultured on uncoated 30% PCL-DA and 30% PCL-DA/VEGF pep scaffolds, and then stimulated to produce phosphorylated VEGF receptor 1 (ph-VEGFR1) or phosphorylated VEGF receptor 2 (ph-VEGFR2). Quantification of phosphorylated VEGFR1 in Fig. 7a showed that HUVECs on 30% PCL-DA scaffolds after 2 h produced a small amount of phosphorylated VEGFR1; HUVECs on the 30% PCL-DA/VEGF pep scaffolds had a slightly higher level of phosphorylated VEGFR1 than that on unfunctionalized scaffolds, yet this difference was not significant and disappeared after 4 h. Testing the phosphorylation of VEGFR2 (Fig. 7b) indicated that both the VEGF peptide signal from the 30% PCL-DA/VEGF pep scaffolds and the addition of soluble VEGF could have a significant effect at 2 h (P ≤ 0.05), which again was not observed after 4 h. Previous studies have confirmed that the VEGF peptide could bind to VRGFR1 and VRGFR2, and activate VRGFR1 and VRGFR1 phosphorylation [21,70]. Webber et al. reported that the effect of VEGF peptide amphiphile on VEGFR1 and VEGFR2 expression was time-dependent, which only increased in the first 10 min, followed by a decrease of stimulation until 60 min [70]. In our experiments, we also see a temporal dependence. Since the cells need some time to attach on functionalized scaffolds and then respond to the VEGF peptide we are likely to see a response time longer than 10 min.

3.10. HUVECs proliferation and morphology on 30% PCL-DA/VEGF pep scaffolds in endothelial growth medium

HUVECs were seeded on uncoated 30% PCL-DA and 30% PCL-DA/VEGF pep scaffolds, and then allowed to proliferate in EGM without VEGF (EGM-VEGF) medium. After 1, 3 and 5 days of culture, cell viability and proliferation were evaluated. As shown in Fig. 8, we consistently noticed an increase in cell viability and DNA content on both scaffolds during culture time. Especially at day 3, cell viability in the 30% PCL-DA/VEGF pep was higher than those of 30% PCL-DA group (Fig. 8a). Moreover, it was noteworthy that DNA content in 30% PCL-DA/VEGF pep scaffold group was significantly higher than 30% PCL-DA scaffold group on day 1 (Fig. 8b). This indicated that VEGF peptide functionalized scaffolds could promote the proliferation of HUVECs. Similar trend was also observed at day 3, which could be attributed to the signal of VEGF peptide resulted from VEGF peptide functionalization. The VEGF peptide we used reproduced the helix region 17–25 of VEGF, which was reported to enhance endothelial cell proliferation by the downstream activation of VEGF dependent intracellular pathway

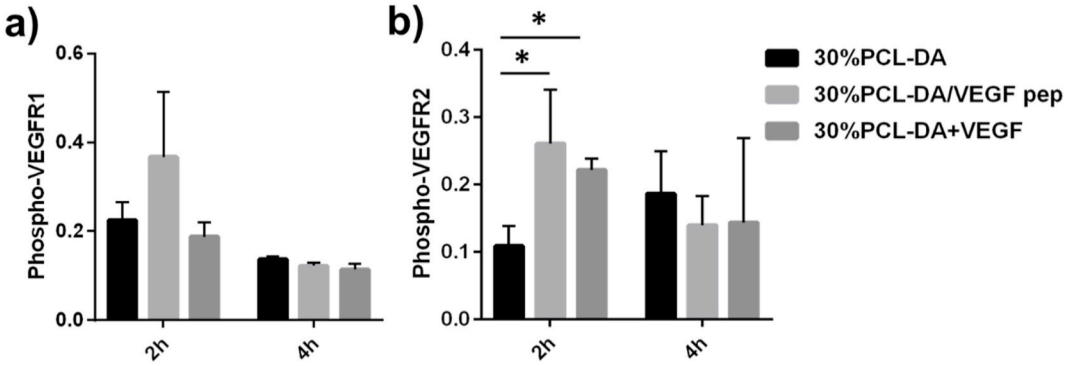

Fig. 7. ELISA analysis of (a) phospho-VEGFR1 and (b) phospho-VEGFR2 production of HUVECs on uncoated 30%PCL-DA and 30% PCL-DA/VEGF pep fibrous scaffolds after 2 h and 4 h "30% PCL-DA + VEGF" represent HUVECs cultured on 30% PCL-DA fibrous scaffolds with adding VEGF in medium. (*P ≤ 0.05; n = 3).

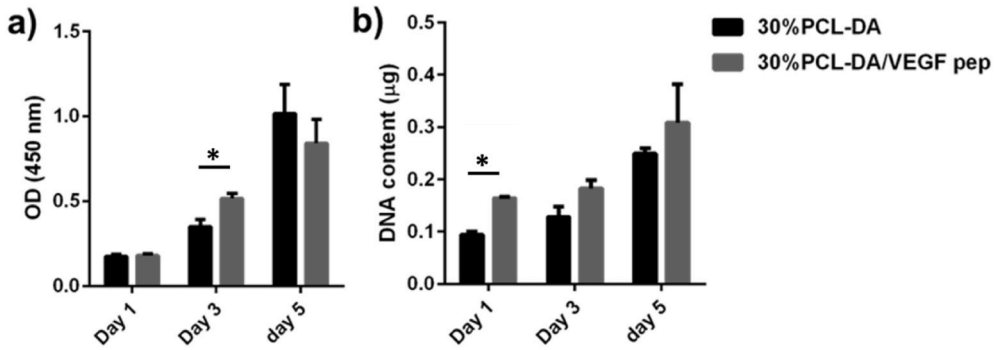

Fig. 8. The viability (a) and proliferation (b) of HUVECs on uncoated 30% PCL-DA and 30% PCL-DA/VEGF pep fibrous scaffolds in EGM medium without VEGF during 5 days of culture. (*P ≤ 0.05; n = 3).

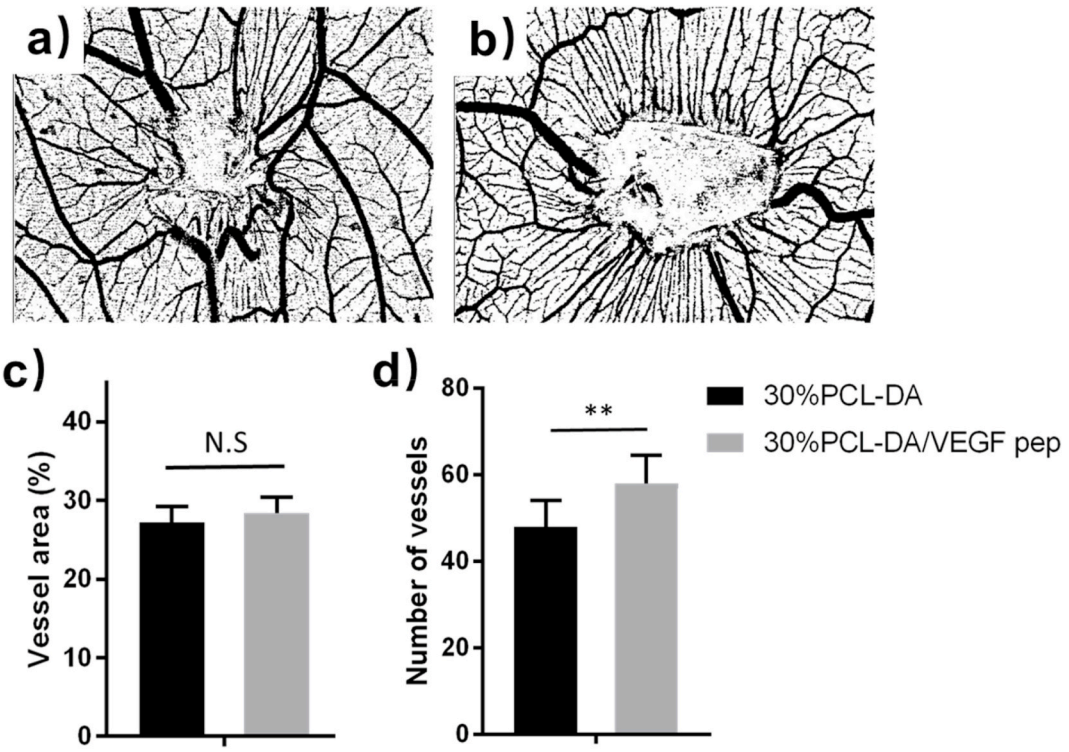

Fig. 9. Processed images of uncoated (a) 30% PCL-DA and (b) 30% PCL-DA/VEGF pep fibrous scaffolds implanted on the CAM after 4 days. The quantification of (c) vessel area in the images and (d) number of vessels around implanted scaffolds. (**P ≤ 0.01; n = 10).

(ERK1/2) [21].

HUVECs were also seeded on coated 30% PCL-DA and 30% PCL-DA/VEGF pep scaffolds to study the effect of VEGF peptide functionalized scaffolds on the proliferation of HUVECs. However, there was no significant difference between 30% PCL-DA and 30% PCL-DA/VEGF pep scaffolds on proliferation during 5 days of culture (Fig. S11). The results indicated that the introduction of Matrigel precoating on scaffolds could cover the signal of VEGF peptide on cell proliferation.

The cell spread and adhesion of HUVECs on different scaffolds was observed by SEM images. Fig. S12 showed the spread of HUVECs on 30% PCL-DA and 30% PCL-DA/VEGF pep scaffold after 3 days of seeding. At 3 days of incubation, most HUVECs attached on the 30% PCL-DA scaffolds remained in a round shape. However, cells on 30% PCL-DA/VEGF pep scaffold exhibited elongated and well-spread morphology. Strong cell adhesion on the surface of 30% PCL-DA/VEGF pep fibers was observed. This finding demonstrated that the functionalization of VEGF peptide on 30% PCL-DA fibers enhanced cell spread and adhesion.

3.11. Cell morphology and expression of endothelial functional proteins on coated scaffolds

In order to observe cell morphology on fibrous scaffolds, DAPI and Phalloidin cell nucleus- and actin filament-staining was performed after 5 days of culture. Results clearly showed that all cells had spread and adhered to both scaffolds. The functional development of HUVECs on coated scaffolds was analyzed by immunostaining of the endothelial proteins, CD31, vWF and eNOS. As seen in Fig. S13, positive CD31 staining was clearly detected on all HUVECs on scaffolds. A vWF dot pattern was observed in small amounts of HUVECs, which demonstrated vWF was produced within the cytoplasm of HUVECs cultured on both scaffolds. eNOS is a marker for nitric oxide production in endothelial cells. All HUVECs stained positive for eNOS, indicating a functional cellular phenotype. Taken together, HUVECs on 30% PCL-DA/VEGF pep scaffolds did not show any considerable visible difference from these immunostaining results as compared to cells seeded on 30% PCL-DA scaffolds. However, cells positively stained with endothelial markers

(CD31, vWF and eNOS) confirmed that HUVECs maintained the endothelial phenotype and kept endothelial function when cultured on both scaffolds.

3.12. In vivo CAM assay

A CAM model was used to evaluate whether the VEGF peptide functionalized scaffolds could promote angiogenesis *in vivo*. After fibrous scaffolds were implanted on the CAM from day 10 until day 14, we saw many vessels growing around electrospun scaffolds as shown in Fig. S14 and Fig. 9a–b. For comparison, the total vessels area and vessels number were quantified (Fig. 9c–d). 30% PCL-DA/VEGF pep fibrous scaffolds displayed a slightly higher (1.2%) amount of vessels area around scaffolds. However, no significant statistical difference compared with 30% PCL-DA fibrous scaffolds was observed ($n = 10$). The quantitative results of vessels number indicated that the number of blood vessels surrounding the 30% PCL-DA/VEGF pep fibrous scaffolds (57.9 ± 6.7) was significantly higher than that of the 30% PCL-DA fibrous scaffolds (48.0 ± 6.0) ($P \leq 0.01$). This means that implantation with 30% PCL-DA/VEGF pep fibrous scaffolds led to more small vessel growth surrounding the scaffolds compared with control. The result suggests a positive angiogenic response from the VEGF peptide functionalized scaffolds *in vivo*.

4. Conclusion

In conclusion, we reported a new approach for the fabrication of VEGF-peptide functionalized electrospun scaffolds by using UV-initiated thiol-ene chemistry. Spatial control of the fiber functionalization, an exclusive advantage of using the photochemically promoted thiol-ene based conjugation strategy, was possible with this set-up. This functionalization approach under mild conditions could maintain fiber morphology and mechanical properties of scaffolds. Moreover, cell studies showed that VEGF peptide functionalized scaffolds significantly enhanced cell survival compared with unfunctionalized scaffolds. Immunostaining images demonstrated that HUVECs could spread, grow and proliferate well, especially maintaining endothelial function on fibrous scaffolds. VEGF peptide functionalized scaffolds enhanced angiogenesis *in vivo* as shown in a CAM assay. The advantages of VEGF peptide-factionalized fibrous scaffolds, especially including the capacity of photopatterning, make them attractive for vascular tissue engineering. Engineered vascular tissue could have potential as the transplantation grafts in the treatment of cardiovascular diseases.

Ethics Approval and Consent to participate

This manuscript is not related to clinical study, and doesn't involve any animal experiments, human data or human tissue. We only performed the chick embryo chorioallantoic membrane (CAM) assay. This model does not require ethics committee approval if embryo stays in the shell.

Ethics Approval and Consent to Participate is not applicable in this submission.

CRediT authorship contribution statement

Tianyu Yao: Conceptualization, Methodology, Investigation, Visualization, Formal analysis, Writing – original draft. **Honglin Chen:** Methodology, Investigation, Visualization, Writing-revision draft, Funding acquisition. **Rong Wang:** Investigation. **Rebeca Rivero:** Investigation, Writing – review & editing. **Fengyu Wang:** Investigation. **Lilian Kessels:** Investigation, Resources. **Stijn M. Agten:** Investigation, Resources. **Tilman M. Hackeng:** Investigation, Resources. **Tim G.A.M. Wolfs:** Investigation, Resources. **Daidi Fan:** Investigation, Resources. **Matthew B. Baker:** Conceptualization, Supervision, Resources, Writing – review & editing, Funding acquisition. **Lorenzo Moroni:** Conceptualization, Supervision, Resources, Writing – review & editing, Funding acquisition.

Declaration of competing interest

The authors declare that they have no known competing financial interests or personal relationships that could have appeared to influence the work reported in this paper.

Acknowledgments

This work was supported in part by China Scholarship Council (No. 201508610081 to T.Y.) and by the National Natural Science Foundation of China (No. 32071360 and No. 31900976 to H.C.) This research project has been made possible thanks to the support of the Dutch Province of Limburg.

Appendix A. Supplementary data

Supplementary data to this article can be found online at https://doi.org/10.1016/j.bioactmat.2022.05.029.

References

[1] L.S. Gambino, N.G. Wreford, J.F. Bertram, P. Dockery, F. Lederman, P.A. Rogers, Angiogenesis occurs by vessel elongation in proliferative phase human endometrium, Human Reproduction 17 (5) (2002) 1199–1206.
[2] R. Munoz-Chapuli, A. Quesada, M.A. Medina, Angiogenesis and signal transduction in endothelial cells, Cellular and Molecular Life Sciences CMLS 61 (17) (2004) 2224–2243.
[3] W. Risau, Mechanisms of angiogenesis, nature 386 (6626) (1997) 671.
[4] M.W. Laschke, Y. Harder, M. Amon, I. Martin, J. Farhadi, A. Ring, N. Torio-Padron, R. Schramm, M. Rücker, D. Junker, Angiogenesis in tissue engineering: breathing life into constructed tissue substitutes, Tissue engineering 12 (8) (2006) 2093–2104.
[5] M. Lovett, K. Lee, A. Edwards, D.L. Kaplan, Vascularization strategies for tissue engineering, Tissue Engineering Part B: Reviews 15 (3) (2009) 353–370.
[6] N. Goonoo, Vascularization and angiogenesis in electrospun tissue engineered constructs: towards the creation of long-term functional networks, Biomedical Physics & Engineering Express 4 (3) (2018), 032001.
[7] J.M. Stenman, J. Rajagopal, T.J. Carroll, M. Ishibashi, J. McMahon, A.P. McMahon, Canonical Wnt signaling regulates organ-specific assembly and differentiation of CNS vasculature, Science 322 (5905) (2008) 1247–1250.
[8] D.W. Hutmacher, Scaffolds in Tissue Engineering Bone and Cartilage, the Biomaterials: Silver Jubilee Compendium, Elsevier, 2000, pp. 175–189.
[9] T.P. Richardson, M.C. Peters, A.B. Ennett, D.J. Mooney, Polymeric system for dual growth factor delivery, Nature biotechnology 19 (11) (2001) 1029.
[10] L. Coultas, K. Chawengsaksophak, J. Rossant, Endothelial cells and VEGF in vascular development, Nature 438 (7070) (2005) 937.
[11] M. Grunewald, I. Avraham, Y. Dor, E. Bachar-Lustig, A. Itin, S. Yung, S. Chimenti, L. Landsman, R. Abramovitch, E. Keshet, VEGF-induced adult neovascularization: recruitment, retention, and role of accessory cells, Cell 124 (1) (2006) 175–189.
[12] W.J. Lamoreaux, M.E. Fitzgerald, A. Reiner, K.A. Hasty, S.T. Charles, Vascular endothelial growth factor increases release of gelatinase A and decreases release of tissue inhibitor of metalloproteinases by microvascular endothelial cellsin vitro, Microvascular research 55 (1) (1998) 29–42.
[13] A. Sahni, C.W. Francis, Vascular endothelial growth factor binds to fibrinogen and fibrin and stimulates endothelial cell proliferation, Blood 96 (12) (2000) 3772–3778.
[14] J. Oswald, S. Boxberger, B. Jørgensen, S. Feldmann, G. Ehninger, M. Bornhäuser, C. Werner, Mesenchymal stem cells can be differentiated into endothelial cells in vitro, Stem cells 22 (3) (2004) 377–384.
[15] N. Ferrara, Molecular and biological properties of vascular endothelial growth factor, Journal of molecular medicine 77 (7) (1999) 527–543.
[16] P. Chames, M. Van Regenmortel, E. Weiss, D. Baty, Therapeutic antibodies: successes, limitations and hopes for the future, British journal of pharmacology 157 (2) (2009) 220–233.
[17] F. Zhou, X. Jia, Y. Yang, Q. Yang, C. Gao, Y. Zhao, Y. Fan, X. Yuan, Peptide-modified PELCL electrospun membranes for regulation of vascular endothelial cells, Materials Science and Engineering: C 68 (2016) 623–631.
[18] L. Cai, C.B. Dinh, S.C. Heilshorn, One-pot synthesis of elastin-like polypeptide hydrogels with grafted VEGF-mimetic peptides, Biomaterials science 2 (5) (2014) 757–765.
[19] F. Finetti, A. Basile, D. Capasso, S. Di Gaetano, R. Di Stasi, M. Pascale, C.M. Turco, M. Ziche, L. Morbidelli, L.D. D'Andrea, Functional and pharmacological characterization of a VEGF mimetic peptide on reparative angiogenesis, Biochemical pharmacology 84 (3) (2012) 303–311.

[20] J.E. Leslie-Barbick, J.E. Saik, D.J. Gould, M.E. Dickinson, J.L. West, The promotion of microvasculature formation in poly (ethylene glycol) diacrylate hydrogels by an immobilized VEGF-mimetic peptide, Biomaterials 32 (25) (2011) 5782–5789.
[21] L.D. D'Andrea, G. Iaccarino, R. Fattorusso, D. Sorriento, C. Carannante, D. Capasso, B. Trimarco, C. Pedone, Targeting angiogenesis: structural characterization and biological properties of a de novo engineered VEGF mimicking peptide, Proceedings of the National Academy of Sciences 102 (40) (2005) 14215–14220.
[22] T.R. Chan, P.J. Stahl, S.M. Yu, Matrix-bound vegf mimetic peptides: design and endothelial-cell activation in collagen scaffolds, Advanced functional materials 21 (22) (2011) 4252–4262.
[23] X. Wang, A. Horii, S. Zhang, Designer functionalized self-assembling peptide nanofiber scaffolds for growth, migration, and tubulogenesis of human umbilical vein endothelial cells, Soft Matter 4 (12) (2008) 2388–2395.
[24] P.J. Stahl, T.R. Chan, Y.I. Shen, G. Sun, S. Gerecht, S.M.J. Yu, Capillary network-like organization of endothelial cells in PEGDA scaffolds encoded with angiogenic signals via triple helical hybridization, Advanced functional materials 24 (21) (2014) 3213–3225.
[25] A. Cheng, Z. Schwartz, A. Kahn, X. Li, Z. Shao, M. Sun, Y. Ao, B.D. Boyan, H. Chen, Advances in porous scaffold design for bone and cartilage tissue engineering and regeneration, Tissue Engineering Part B: Reviews 25 (1) (2019) 14–29.
[26] J.D. Kretlow, A.G. Mikos, From material to tissue: biomaterial development, scaffold fabrication, and tissue engineering, AIChE Journal 54 (12) (2008) 3048–3067.
[27] S. Ramakrishna, K. Fujihara, W.-E. Teo, T. Yong, Z. Ma, R. Ramaseshan, Electrospun nanofibers: solving global issues, Materials today 9 (3) (2006) 40–50.
[28] W.J. Li, C.T. Laurencin, E.J. Caterson, R.S. Tuan, F.K. Ko, Electrospun nanofibrous structure: a novel scaffold for tissue engineering, Journal of Biomedical Materials Research: An Official Journal of The Society for Biomaterials 60 (4) (2002) 613–621. The Japanese Society for Biomaterials, and The Australian Society for Biomaterials and the Korean Society for Biomaterials.
[29] J. Kucinska-Lipka, I. Gubanska, H. Janik, M. Sienkiewicz, Fabrication of polyurethane and polyurethane based composite fibres by the electrospinning technique for soft tissue engineering of cardiovascular system, Materials Science and Engineering: C 46 (2015) 166–176.
[30] Z.-M. Huang, Y.-Z. Zhang, M. Kotaki, S. Ramakrishna, A review on polymer nanofibers by electrospinning and their applications in nanocomposites, Composites science and technology 63 (15) (2003) 2223–2253.
[31] N. Bhardwaj, S.C. Kundu, Electrospinning: a fascinating fiber fabrication technique, Biotechnology advances 28 (3) (2010) 325–347.
[32] R. Murugan, S. Ramakrishna, Nano-featured scaffolds for tissue engineering: a review of spinning methodologies, Tissue engineering 12 (3) (2006) 435–447.
[33] Q.P. Pham, U. Sharma, A.G. Mikos, Electrospinning of polymeric nanofibers for tissue engineering applications: a review, Tissue engineering 12 (5) (2006) 1197–1211.
[34] Y. Yang, Q. Yang, F. Zhou, Y. Zhao, X. Jia, X. Yuan, Y. Fan, Electrospun PELCL membranes loaded with QK peptide for enhancement of vascular endothelial cell growth, Journal of Materials Science: Materials in Medicine 27 (6) (2016) 1–10.
[35] S. Stojanov, A. Berlec, Electrospun nanofibers as carriers of microorganisms, stem cells, proteins, and nucleic acids in therapeutic and other applications, Frontiers in bioengineering and biotechnology 8 (2020) 130.
[36] H.S. Yoo, T.G. Kim, T.G. Park, Surface-functionalized electrospun nanofibers for tissue engineering and drug delivery, Advanced drug delivery reviews 61 (12) (2009) 1033–1042.
[37] S.Y. Chew, J. Wen, E.K. Yim, K.W. Leong, Sustained release of proteins from electrospun biodegradable fibers, Biomacromolecules 6 (4) (2005) 2017–2024.
[38] F. Costa, I.F. Carvalho, R.C. Montelaro, P. Gomes, M.C.L. Martins, Covalent immobilization of antimicrobial peptides (AMPs) onto biomaterial surfaces, Acta biomaterialia 7 (4) (2011) 1431–1440.
[39] S.G. Lévesque, M.S. Shoichet, Synthesis of cell-adhesive dextran hydrogels and macroporous scaffolds, Biomaterials 27 (30) (2006) 5277–5285.
[40] S. Xiao, M. Textor, N.D. Spencer, M. Wieland, B. Keller, H. Sigrist, Immobilization of the cell-adhesive peptide Arg–Gly–Asp–Cys (RGDC) on titanium surfaces by covalent chemical attachment, Journal of materials science: Materials in Medicine 8 (12) (1997) 867–872.
[41] X. Duan, C. McLaughlin, M. Griffith, H. Sheardown, Biofunctionalization of collagen for improved biological response: scaffolds for corneal tissue engineering, Biomaterials 28 (1) (2007) 78–88.
[42] A.S. Sarvestani, X. He, E. Jabbari, Effect of osteonectin-derived peptide on the viscoelasticity of hydrogel/apatite nanocomposite scaffolds, Biopolymers: Original Research on Biomolecules 85 (4) (2007) 370–378.
[43] O.I. Kalaoglu-Altan, B. Verbraeken, K. Lava, T.N. Gevrek, R. Sanyal, T. Dargaville, K. De Clerck, R. Hoogenboom, A. Sanyal, Multireactive poly (2-oxazoline) nanofibers through electrospinning with crosslinking on the fly, ACS Macro Letters 5 (6) (2016) 676–681.
[44] W.H. Binder, R. Sachsenhofer, 'Click'chemistry in polymer and materials science, Macromolecular Rapid Communications 28 (1) (2007) 15–54.
[45] A. Celebioglu, S. Demirci, T. Uyar, Cyclodextrin-grafted electrospun cellulose acetate nanofibers via "Click" reaction for removal of phenanthrene, Applied Surface Science 305 (2014) 581–588.
[46] J.E. Moses, A.D. Moorhouse, The growing applications of click chemistry, Chemical Society Reviews 36 (8) (2007) 1249–1262.
[47] A.R. Davis, J.A. Maegerlein, K.R. Carter, Electroluminescent networks via photo "click" chemistry, Journal of the American Chemical Society 133 (50) (2011) 20546–20551.
[48] A. Lancuški, S.b. Fort, F.d.r. Bossard, Electrospun azido-PCL nanofibers for enhanced surface functionalization by click chemistry, ACS applied materials & interfaces 4 (12) (2012) 6499–6504.
[49] Q. Shi, X. Chen, T. Lu, X. Jing, The immobilization of proteins on biodegradable polymer fibers via click chemistry, Biomaterials 29 (8) (2008) 1118–1126.
[50] L.A.S. Callahan, S. Xie, I.A. Barker, J. Zheng, D.H. Reneker, A.P. Dove, M.L. Becker, Directed differentiation and neurite extension of mouse embryonic stem cell on aligned poly (lactide) nanofibers functionalized with YIGSR peptide, Biomaterials 34 (36) (2013) 9089–9095.
[51] J. Zheng, K. Liu, D.H. Reneker, M.L. Becker, Post-assembly derivatization of electrospun nanofibers via strain-promoted azide alkyne cycloaddition, Journal of the American Chemical Society 134 (41) (2012) 17274–17277.
[52] O.I. Kalaoglu-Altan, R. Sanyal, A. Sanyal, Clickable" polymeric nanofibers through hydrophilic–hydrophobic balance: fabrication of robust biomolecular immobilization platforms, Biomacromolecules 16 (5) (2015) 1590–1597.
[53] H. Yang, Q. Zhang, B. Lin, G. Fu, X. Zhang, L. Guo, Thermo-sensitive electrospun fibers prepared by a sequential thiol-ene click chemistry approach, Journal of Polymer Science Part A: Polymer Chemistry 50 (20) (2012) 4182–4190.
[54] O.I. Kalaoglu-Altan, R. Sanyal, A. Sanyal, Reactive and 'clickable'electrospun polymeric nanofibers, Polymer Chemistry 6 (18) (2015) 3372–3381.
[55] L. Wang, M. Zhao, S. Li, U.J. Erasquin, H. Wang, L. Ren, C. Chen, Y. Wang, C. Cai, Click" immobilization of a VEGF-mimetic peptide on decellularized endothelial extracellular matrix to enhance angiogenesis, ACS applied materials & interfaces 6 (11) (2014) 8401–8406.
[56] F.C. de Oliveira, D. Olvera, M.J. Sawkins, S.-A. Cryan, S.D. Kimmins, T.E. da Silva, D.J. Kelly, G.P. Duffy, C. Kearney, A.J.B. Heise, in: Direct UV-Triggered Thiol–Ene Cross-Linking of Electrospun Polyester Fibers from Unsaturated Poly (Macrolactone) S and Their Drug Loading by Solvent Swelling, vol. 18, 2017, pp. 4292–4298, 12.
[57] F. Ruiter, L. Sidney, K. Kiick, J. Segal, C. Alexander, F.J.B.s. Rose, The Electrospinning of a Thermo-Responsive Polymer with Peptide Conjugates for Phenotype Support and Extracellular Matrix Production of Therapeutically Relevant Mammalian Cells, vol. 8, 2020, pp. 2611–2626, 9.
[58] P. Viswanathan, E. Themistou, K. Ngamkham, G.C. Reilly, S.P. Armes, G.J. B. Battaglia, Controlling Surface Topology and Functionality of Electrospun Fibers on the Nanoscale Using Amphiphilic Block Copolymers to Direct Mesenchymal Progenitor Cell Adhesion, vol. 16, 2015, pp. 66–75, 1.
[59] M. SCHNölzer, P. Alewood, A. Jones, D. Alewood, S.B.J. Kent, p. research, In Situ Neutralization in Boc-chemistry Solid Phase Peptide Synthesis: Rapid, High Yield Assembly of Difficult Sequences, vol. 40, 1992, pp. 180–193, 3-4.
[60] D. Sharma, B.K. Satapathy, Optimization and physical performance evaluation of electrospun nanofibrous mats of PLA, PCL and their blends, Journal of Industrial Textiles (2020), 1528083720944502.
[61] L. Cai, S. Wang, Poly (ε-caprolactone) acrylates synthesized using a facile method for fabricating networks to achieve controllable physicochemical properties and tunable cell responses, Polymer 51 (1) (2010) 164–177.
[62] Y.-L. Cheng, F. Chen, Preparation and characterization of photocured poly (ε-caprolactone) diacrylate/poly (ethylene glycol) diacrylate/chitosan for photopolymerization-type 3D printing tissue engineering scaffold application, Materials Science and Engineering: C 81 (2017) 66–73.
[63] H. Kweon, M.K. Yoo, I.K. Park, T.H. Kim, H.C. Lee, H.-S. Lee, J.-S. Oh, T. Akaike, C.-S. Cho, A novel degradable polycaprolactone networks for tissue engineering, Biomaterials 24 (5) (2003) 801–808.
[64] J. Tao, S. Shivkumar, Molecular weight dependent structural regimes during the electrospinning of PVA, Materials letters 61 (11–12) (2007) 2325–2328.
[65] S. Eichhorn, W. Sampson, Relationships between specific surface area and pore size in electrospun polymer fibre networks, Journal of The Royal Society Interface 7 (45) (2010) 641–649.
[66] H. Tavanai, R. Jalili, M. Morshed, Effects of fiber diameter and CO2 activation temperature on the pore characteristics of polyacrylonitrile based activated carbon nanofibers, Surface and Interface Analysis, An International Journal devoted to the development and application of techniques for the analysis of surfaces, interfaces and thin films 41 (10) (2009) 814–819.
[67] S.A. Fisher, A.E. Baker, M.S.J. Shoichet, Designing Peptide and Protein Modified Hydrogels: Selecting the Optimal Conjugation Strategy, vol. 139, 2017, pp. 7416–7427, 22.
[68] S. Jalali, M. Tafazzoli-Shadpour, N. Haghighipour, R. Omidvar, F. Safshekan, Regulation of endothelial cell adherence and elastic modulus by substrate stiffness, Cell communication & adhesion 22 (2–6) (2015) 79–89.
[69] P.A. Janmey, D.A. Fletcher, C.A. Reinhart-King, Stiffness sensing by cells, Physiological reviews 100 (2) (2020) 695–724.
[70] M.J. Webber, J. Tongers, C.J. Newcomb, K.-T. Marquardt, J. Bauersachs, D. W. Losordo, S.I. Stupp, Supramolecular nanostructures that mimic VEGF as a strategy for ischemic tissue repair, Proceedings of the National Academy of Sciences 108 (33) (2011) 13438–13443.